# Electrochemical Preparation and Characterization of the Radical Salts of (Phthalocyaninato)nickel, $NiPc(SbF_6)_{0.5}$, and $NiPc(AsF_6)_{0.5}$

Kyuya YAKUSHI,*,† Hideo YAMAKADO, Michiko YOSHITAKE, Nobuhiro KOSUGI, Haruo KURODA, Tadashi SUGANO,†† Minoru KINOSHITA,†† Atsushi KAWAMOTO,††† and Jiro TANAKA†††

Department of Chemistry, Faculty of Science, the University of Tokyo, Hongo, Tokyo 113
††Institute for Solid State Physics, the University of Tokyo, Roppongi, Tokyo 106
†††Department of Chemistry, Faculty of Science, Nagoya University, Furocho, Chikusa-ku, Nagoya 464
(Received September 5, 1988)

The single crystals of $NiPc(SbF_6)_{0.5}$ and $NiPc(AsF_6)_{0.5}$ were prepared by means of an electrochemical method. The electrical, magnetic, optical, and structural properties of these crystals were examined. These crystals are isostructural to each other, and exhibit a metallic behavior at least above 200 K. The *g*-values of the ESR signals remarkably depend upon temperature. By the aid of the low temperature experiments of XANES and reflectance spectrum, the temperature dependence is explained by the model based on the interaction between the small amount of local spins on the Ni atoms and the conduction electrons on the ligand chain. In addition, a sample dependence was found on the ESR properties of the crystals of $NiPc(AsF_6)_{0.5}$. This is attributed to the sample dependence of the concentration of the local spins on Ni atoms. From these considerations, we concluded that the ligand part is mainly oxidized in these partially oxidized salts, in other words the conduction electrons are located on the ligand chain. The bandwidth of the conduction band was estimated to be about 1 eV.

The one-dimensional metals based on the metal phthalocyanine (MPc) or metal tetrabenzoporphyrin (MTBP) are unique materials which may be able to involve two conduction pathways in the same metal macrocycle column.[1] These pathways are possibly composed of the $\pi$-orbital of the ligand and the $d_{z^2}$-orbital of the central metal, first because the molecules are stacking with the overlapping mode of a metal-over-metal type,[2] secondly because the highest occupied molecular orbital (HOME) of a phth alocyanine (Pc) does not mix with the $d_{z^2}$-orbital of the central metal due to the symmetry restriction, thirdly because their orbital energies are quite close.[3-5] The excitonic superconducting mechanism is theoretically proposed in the materials which involve this kind of composite energy bands that are weakely coupled and proximately located to each other.[6] Therefore, it is of great importance to elucidate which orbitals are contributing to make the conduction bands. The research group at Northwestern University extensively studied the partially oxidized salts of metal phthalocyanine (MPc) and metal tetrabenzoporphyrin (MTBP).[1,2,7-14] As for the iodine complex (NiPcI) of NiPc, the conduction band is formed from the highest occupied molecular orbital (HOMO, $a_{1u}$) of the Pc ligand, and the d-orbital is not involved in the conduction band.[2] On the other hand, the conduction electrons of CoPcI are located on the metal chain in the Pc column.[10] Furthermore, the unpaired electrons of the iodine complex (NiTBPI) of NiTBP exhibit that they are located partly at the ligand site and partly at the Ni site.[1] Martinsen et al. interpreted this phenomenon by considering that the conduction band is composed of $a_{1g}(3d_{z^2})$-band along the metal chain and the $a_{1u}(\pi)$-band along the ligand chain.[1] We prepared the analogous complexes, $NiPc(SbF_6)_{0.5}$ and $NiPc(AsF_6)_{0.5}$, by the use of the electrochemical oxidation of NiPc, and found that the ESR behavior of $NiPc(SbF_6)_{0.5}$ is quite similar to that of NiTBPI.[15,16] Later on, we found a strong sample dependence on the ESR property of $NiPc(AsF_6)_{0.5}$. Lookig at this phenomenon through the eyes of ESR, some crystals of $NiPc(AsF_6)_{0.5}$ behave like NiPcI, someone like CoPcI, and the others like NiTBPI. We are interested in whether the conduction band of $NiPc(SbF_6)_{0.5}$ is really composed of the $\pi$-and $d_{z^2}$-orbitals, and whether the sample dependence of $NiPc(AsF_6)_{0.5}$ is the intrinsic property. In this paper, we present the experimental results on the temperature dependence of the ESR property, XANES and reflectance spectrum of $NiPc(SbF_6)_{0.5}$, and characterize the magnetically different $NiPc(AsF_6)_{0.5}$ by means of EPMA, X-ray diffraction, and reflectance spectrum.

## Experimental

The finely powdered NiPc was refluxed in the pyridine solution and was filtrated to remove CoPc. This procedure was repeated over ten times and then the filtrated NiPc powder was sublimed in vacuum for four times. The contamination by the magnetic impurity was less than $10^{-4}$ spins per a NiPc molecule which was estimated with the aid of ESR at low temperature. The ESR signal of this impurity, probably $Co^{2+}$ species, was not attributed to CoPc, since the ESR pattern due to the hyperfine splitting was entirely different from that of CoPc.[17] $(n\text{-Bu})_4NSbF_6$ and $(n\text{-Bu})_4NAsF_6$ which were used as electrolytes for the electrochemical oxidation were prepared by mixing the equimolar aqueous solutions of $(n\text{-Bu})_4NBr$ and $NaSbF_6$ or $KAsF_6$. The precipitated $(n\text{-Bu})_4NSbF_6$ and $(n\text{-Bu})_4NAsF_6$ were recrystallized from the methanol solution for three times. 1-chloronaphthalene was refluxed with $CaH_2$ and purified by vacuum distillation. The radical salts of NiPc were prepared by the method of electrochemical crystallization at 120±2 °C under the Ar

† Present address: Institute for Molecular Science, Myodaiji-cho, Okazaki, Aichi 444.

atmosphere. The concentrations of the electrolyte and NiPc were $2.5\times10^{-3}$ and $3\times10^{-4}$ mol $l^{-1}$, respectively. The crystals were grown for about two weeks with a galvanostatic mode of 2 $\mu$A.

The chemical analysis of Ni, Sb, and As were conducted with the aid of ICP atomic emission spectroscopy. Several single crystals (ca. 10 $\mu$g) were dissolved in concd $H_2SO_4$, then decomposed in concd $HNO_3$ and diluted with pure water. The emission lines, 231.6, 206.8, and 193.6 nm were used for the detection of Ni, Sb, and As. The intensities of these emission lines were measured simultaneously by using Jarrel-Ash, Model Plasma Atomcomp MK-II. The atomic ratios were Sb/Ni=0.48±0.04 for NiPc-$SbF_6$ and As/Ni=0.50±0.02 for NiPc-$AsF_6$. The sample dependence of the atomic ratio between Ni and As of the single crystal was measured by means of EPMA using JEOL superprobe 733. The Ni foil and the single crystal of GaAs were used as the standard materials of Ni and As atoms. EPMA were performed at seven points on each crystal of 0.03 mm×0.03 mm×0.3 mm by the use of the electron beam of 1 $\mu$m diameter.

ESR was measured on a needle-like single crystal or a bundle of single crystals using JEOL JES-FE1XG combined with an Air Products LTR-3-110 continuous flow type liquid He cryostat. The needle-like crystals over 10 were aligned in the Pyrex capillary. Li-TCNQ was used as the standard sample to determine the $g$-value. The intensity of the ESR signal was calculated by the numerical double integration, and this intensity was transformed to the spin susceptibility by the comparison with the intensity of the ESR signal of violanthrone for which the static susceptibility had been measured.

For the experiment of X-ray diffraction, we used the needle-like crystal of $NiPc(AsF_6)_{0.5}$ developing along the c-axis, the typical dimension of which was 0.05 mm×0.05 mm×0.5 mm. The 2296 reflections were collected using Rigaku four-circle automated diffractometer. The X-ray source was the Cu $K\alpha$ radiation monochromatized with a graphite plate. We selected 1940 reflections which are three times larger than the standard deviations estimated from the counting errors. The absorption correction was made with a program ACACA written by Prewitt. The structure was solved by the heavy atom method and was refined by the block-diagonal least-squares method with the anisotropic temperature factors for Ni, N, C, As, and F atoms and the isotropic temperature factors for H atoms. The possible space group was *Pncm* or *Pnc*2 from the systematic absence. At first the structure was analyzed assuming the space group, *Pncm*. However, the final $R$-value was 0.12, and the temperature factors of F atoms were too large. This means that F atoms are neither located on the mirror plane nor two-fold axis. Thus, the structure was analyzed in the non-centrosymmetric space group, *Pnc*2. The final $R$-value was 0.065.

The X-ray absorption spectrum near the Ni K-edge was measured using the EXAFS facilities at the beam line 10B of the Photon Factory in the National Laboratory for High Energy Physics (KEK-PF).[18] The single crystal of the dimension, 0.15 mm×0.15 mm×2 mm, was used for measuring the transmission spectrum. This crystal was fixed with vacuum grease onto the round mask which was made from stainless steel with the thickness of 0.1 mm, and had a rectangular diaphragm of 0.1 mm×1 mm. Polarized spectra were measured with the X-ray polarization parallel, 45°, and perpendicular to the long axis of the crystal. The CTi cryocooler, Model 20, was used for cooling the sample crystal.

The polarized reflectance spectra of single crystals were measured at room temperature and 80 K using the micro-spectro-reflectometer which was designed and constructed in our laboratory (Chemistry Department, the University of Tokyo).[19]

Temperature dependence of the electrical resistivity was measured by the low-frequency AC four-probe method. The electrical contact to the 10 $\mu$m gold wires was made with carbon paint. The cooling rate of the crystal was about 0.5 K $min^{-1}$.

## Results and Discussion

**$NiPc(SbF_6)_{0.5}$.** The chemical ratio between NiPc and $SbF_6$ is consistent with the crystal structure which we have published in the previous paper.[15] The crystal belongs to the orthorhombic system, the space group being *Pnc*2. The lattice constants are $a$=14.113(1) Å, $b$=28.710(2) Å, $c$=6.441(2) Å, and $Z$=2. The crystal structure is essentially the same as that of $NiPc(AsF_6)_{0.5}$, the structural details of which will be described in the next section. NiPc is stacking metal-over-metal with the planes of molecules normal to the stacking axis. Successive molecules are staggered by 41.0°. The unit cell contains two molecular columns. The counter anions, $SbF_6^-$, are located on the same plane of NiPc, so that NiPc is pushed away by 0.2 Å from the stacking axis. Therefore, the metal chain of NiPc is aligned zigzag along the c-axis. Unlike the disordered arrangement of $I_3^-$ in the NiPcI crystal,[2] $SbF_6^-$ is three dimensionally ordered in this material. However, they are probably thermally fluctuating since the temperature factors of anion is larger by a factor of 5—10 than those of NiPc.[15]

The electrical conductivity is 10—200 S $cm^{-1}$ at room temperature and gradually increases on lowering temperature down to 250 K. At lower temperature, however, the resistivity jumps take place at various temperatures, which are not reproducible in the heating or cooling processes. Therefore, the intrinsic behavior of the electrical resistivity in the low temperature region is unidentified at present. Since these resistivity jumps are sometimes observed in the one-dimensional materials, this phenomenon indicates the one-dimensional electric conduction in this material.

The angle dependence of the $g$-value at room temperature was showm in Fig. 1. The principal values are $g_{/\!/}$=1.994 and $g_{\perp}$=2.030, where // and ⊥ denote the geometrical relation between the c-axis of the crystal and the static magnetic field. These axes just coincide with the principal axes of the NiPc molecule. The principal values of NiPc molecule are

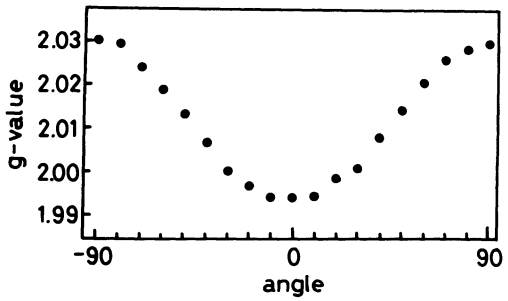


Fig. 1. Angular dependence of the g-value of $NiPc(SbF_6)_{0.5}$. The c-axis is parallel to the static magnetic field when the angle is 0°.

$g_{/\!/}$=2.113 and $g_\perp$=2.292 for metal-oxidized species, $Ni^{3+}Pc^{2-}$, and $g_{/\!/} \sim g_\perp$=2.003 for ligand-oxidized species, $Ni^{2+}Pc^{-}$.[20] Therefore the unpaired electrons of $NiPc(SbF_6)_{0.5}$ has an intermediate character between the metal-oxidized $Ni^{3+}Pc^{2-}$ and the ligand-oxidized $Ni^{2+}Pc^{-}$. This character of the unpaired electrons show a contrast to the $\pi$-character of NiPcI, in which the principal values are $g_{/\!/}$=2.0075, $g_\perp$=2.0007.[2] Martinsen et al. found the intermediate g-values ($g_{/\!/}$=2.060 and $g_\perp$=2.018) in NiTBPI, and attributed them to the rapid transfer of the unpaired electron between a ligand and a central metal.[1] Therefore, a similar situation is possibly realized in $NiPc(SbF_6)_{0.5}$. The relation, $g_{/\!/} > g_\perp$, which is reverse to the usual square planar $d^7$ complex with a low spin configuration, was explained on the basis of the back charge transfer from triiodide ion. In this sense, the contrary relation, $g_{/\!/} < g_\perp$, in this crystal is consistent with their interpretation, because this material does not contain triiodide ions. At the same time, the angular dependence of the g-value indicates that the ESR signal is originated from the $Ni^{3+}Pc^{2-}$ species in the crystal, and suggests that the d-hole configuration of $Ni^{3+}Pc^{2-}$ is $(d_{x^2-y^2})^2(d_{z^2})^1$.[21]

The temperature dependence of ESR were conducted on ca. 20 single crystals aligned in the glass capillary so that the needle axes (//c) were perpendicular to the static magnetic field. The temperature dependence of $g_\perp$, a linewidth, and a doubly integrated intensity were displayed in Figs. 2b—2d. With the decrease of temperature,the linewidth and $g_\perp$ remarkably increase and the intensity slightly decreases. The increase of the linewidth is closely related to the increase of $g_\perp$ which is the measure of the contribution of d-orbital which brings about the fast relaxation due to the large spin-orbit coupling constant. The temperature-dependent spin susceptibility was divided into two components, one of which comes from the metal chain and the other from the ligand chain using the following equation.[22]

$$\chi_{Ni}(T) = [(g_{obs} - g_{Pc})/(g_{Ni} - g_{Pc})]\chi_{obs}(T)$$
$$\chi_{Pc}(T) = [(g_{Ni} - g_{obs})/(g_{Ni} - g_{Pc})]\chi_{obs}(T)$$

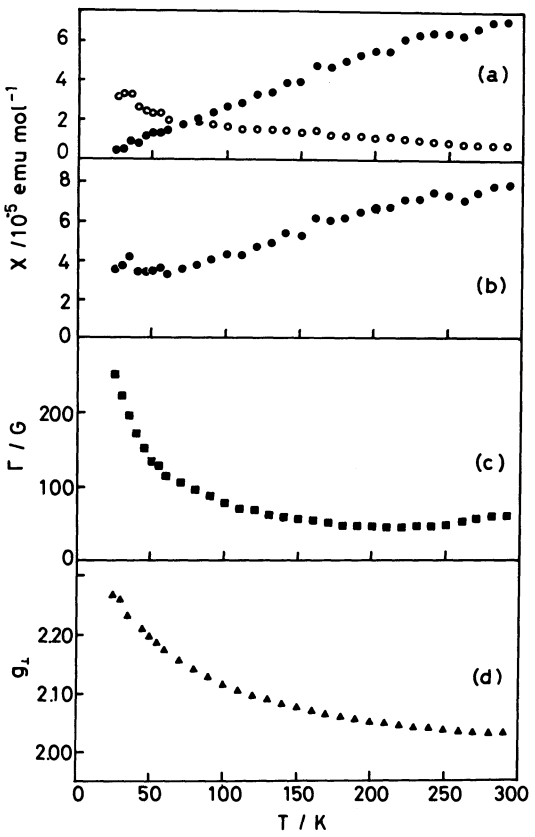


Fig. 2. Temperature dependence of the ESR signal (H⊥c) of $NiPc(SbF_6)_{0.5}$. (a) Spin susceptibilities of the Ni chain (open circle) and the Pc chain (solid circle), (b) observed spin susceptibility, (c) linewidth, and (d) g-value.

These results are drawn by solid and open circles in Fig. 2a. In this process, we tentatively used $g_{Ni}$=2.292 and $g_{Pc}$=2.003 which were reported by Bobrovskii and Sidorov in the oleum solution of NiPc.[20] The $g_\perp$ of $NiPc(SbF_6)_{0.5}$ is in-between those of $Ni^{3+}Pc^{2-}$ and $Ni^{2+}Pc^{-}$, but the $g_{/\!/}$ is smaller than both of them. It is well-known that the g-values of the transition metal atoms coordinated with a square planar mode are very sensitive to the axial coordination by the solvent molecule. In fact as we will mention in the next section, the $g_\perp$-value of some crystals of $NiPc(AsF_6)_{0.5}$ is larger than $g_\perp$=2.292 of $Ni^{3+}Pc^{2-}$. Therefore, the larger values than 2.292 should be taken as the standard g-value of a metal-oxidized species. Taking this situation into account, the contribution of $\chi_{Ni}(T)$ is overestimated in this analysis, but we believe that the qualitative trend on temperature dependence is reliable. At low temperature, $\chi_{Ni}(T)$ increases and overwhelms $\chi_{Pc}(T)$ which is dominant at room temperature.

Martinsen et al. studied the structure and properties of NiTBPI, which exhibits quite similar ESR properties to that of $NiPc(SbF_6)_{0.5}$.[2] They qualitatively interpreted the d-character of the unpaired electrons using the

band model composed of the two conduction bands, one of which derived from the HOMO of the ligand ($a_{1u}$-band) and the other from the $3d_{z^2}$ orbital of a Ni atom ($a_{1g}$-band). They regarded the $a_{1g}$-band as the origin of the d-character. The conduction electrons in the $a_{1u}$ and $a_{1g}$ bands exchange with each other faster than the microwave frequency. In this model a considerable amount of charge carriers are located on the conducting Ni chain as well as on the conducting Pc chain. However, it is not easy to explain the temperature dependence of the $g$-value by this model. For example, the contribution of $\chi_{Pc}(T)$ is dominant at room temperature, but it is reverse at low temperature as shown in Fig. 2a. To explain this behavior based on the Pauli paramagnetism of the two tight-binding bands, we have to shift the relative position of these band centers depending upon the temperature so as to adjust the density of state at the Fermi level of each band. This requires the temperature dependent band filling factor, namely the degrees of oxidation at the Ni and ligand sites. Another possible interpretation is based on the model in which the conduction electrons are located mainly on the ligands and they exchange rapidly with a small amount of localized electrons on the Ni sites. This is the extreme case where the bandwidth of the d-band is much narrower than that of $\pi$-band. In this model, the increase of $\chi_{Ni}(T)$ is attributed to the Curie law, and the decrease of $\chi_{Pc}(T)$ is related to a narrow energy gap in the conduction band, which will be discussed again in the next section. Assuming the Curie law as to $\chi_{Ni}(T)$, the spin concentration at the Ni site with $S=1/2$ was estimated to be $4\times10^{-3}$ spins per a NiPc. Therefore, the ligand site is predominantly oxidized, so that the temperature dependent degree of oxidation at the ligand site is not necessary in this model. These two models can be distinguished from the temperature dependence of the numbers of charge carriers on each chain. If the degree of oxidation on each chain does change at low temperature, we have to adopt the former model, while the latter model will be appropriate if not. The temperature dependence of the d-holes at the Ni site is examined with the X-ray absorption spectrum of 1s→3d transition, and the change of the degree of oxidation at Pc site at low temperature is checked by the intensity of the Q-band.

The X-ray absorption spectrum of the electron quadrupole transition, 1s→3d, provides the information on the bulk property of the vacant d-orbitals. The spectra (1) and (2) shown in Fig. 3 are the X-ray absorption spectra near the K-edge on the powdered samples of $NiPc(SbF_6)_{0.5}$ and NiPc, respectively. As for the 1s→3d transition at 8321.5 eV, no significant difference was found between them. The spectra (3), (4), and (5) in Fig. 3 are the polarized absortion spectra of the 1s→3d quadrupole transition of the single crystal of $NiPc(SbF_6)_{0.5}$. The selection rule of the

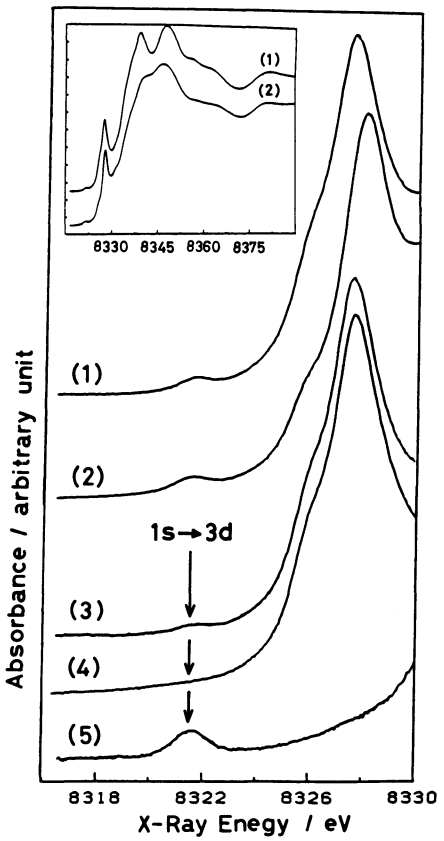


Fig. 3. X-Ray absorption spectra of the powdered samples of (1) $(NiPc)_2SbF_6$ and (2) NiPc, and (3—5) the single crystals of $NiPc(SbF_6)_{0.5}$. A weak absorption band at about 8321.5 eV is the 1s→3d electric quadrupole transition, and the absorption band at about 8328 eV is the electric dipole 1s→$\pi^*$ transition. (3) The electric vector makes an angle of 45° with the c-axis in the polarization plane. (4) The electric vector of the incident light is parallel to the c-axis. (5) The polarization plane of the incident light is perpendicular to the c-axis.

quadrupole transition is determined by the relative direction between the one-dimensional Ni chain and the polarization plane (the plane of vibration of electric field).[23] The selection rule of the 1s to 3d transition is listed in Table 1. If this absorption band is a single component, this transition is assigned to the 1s→$3d_{x^2-y^2}$ from the selection rule and the theoretical study of the NiPc free molecule.[5] This experimental result apparently indicates that the d-orbitals except $3d_{x^2-y^2}$ is fully occupied as expected in the second model. However, the interpretation of this spectrum is not simple, because CoPc and FePc also exhibited a single absorption band for the 1s→3d transition,[24] although they have respectively the electronic configurations of $(3d)^7$ and $(3d)^6$. Therefore, we cannot preclude the possibility that 1s→3d band of $NiPc(SbF_6)_{0.5}$ is attributed to the superposition of the 1s→$3d_{x^2-y^2}$ transition and the other 1s→3d transition. This case is consistent with the first model (two-band model). If

Table 1. Selection Rule of Quadrupole Transition

(1) E⊥c: When the c-axis of the crystal is perpendicular to the polarization plane, a quadrupole transition is allowed only from 1s to $3d_{x^2-y^2}$ and to $3d_{xy}$. (2) E//c: When the electric vector is parallel to the c-axis, quadrupole transition is allowed from 1s to $3d_{xy}$ and $3d_{yz}$. (3) ∠(E,c)=45°: When the c-axis makes an angle of 45° against the electric field vector in the polarization plane, the transition from 1s to $3d_{z^2}$ and $3d_{x^2-y^2}$ is allowed.

| | $d_{x^2-y^2}$ | $d_{z^2}$ | $d_{xy}$ | $d_{xz}$ | $d_{yz}$ | Experimental |
|---|---|---|---|---|---|---|
| (1) | O | × | O | × | × | Observed |
| (2) | × | × | × | O | O | Not observed |
| (3) | O | O | × | × | × | Observed |

O: allowed transition, ×: forbidden transition.

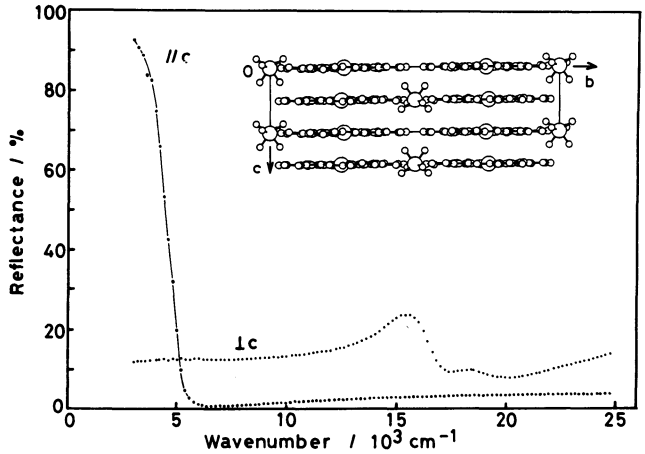


Fig. 4. Polarized reflectance spectrum of the single crystal of $(NiPc)_2SbF_6$. The inset shows the crystal structure of $(NiPc)_2SbF_6$.

this is the case, the candidate of this vacant d-orbital is $3d_{z^2}$ or $3d_{xy}$ from the selection rule shown in Table 1, and then the $1s \rightarrow 3d_{z^2}$ or $1s \rightarrow 3d_{xy}$ transition should change significantly at low temperature accompanying the change of the degree of oxidation at the Ni site. However, no significant change was detected in the 50 K spectra of the powdered sample and the single crystal. This result supports the second model, that is, the majority of carriers are located on the ligand chain and a small amount of unpaired electrons are localized at the Ni site. The d-character of the ESR signal is attributable to the rapid exchange between these local spins at the Ni site and the migrating spins on the ligand chain. Figure 4 shows the polarized reflectance spectrum of the single crystal of $NiPc(SbF_6)_{0.5}$. In the ⊥c spectrum, the intramolecular transition (Q-band) of a neutral NiPc was observed at 15400 $cm^{-1}$. Figure 5 shows the comparison of the ⊥c spectra at room temperature and 80 K. In this spectrum, weak shoulders showed up around 13000 and 23000 $cm^{-1}$. These weak dispersions are tentatively assigned to the intramolecular transitions of $Ni^{2+}Pc^-$ cation radical

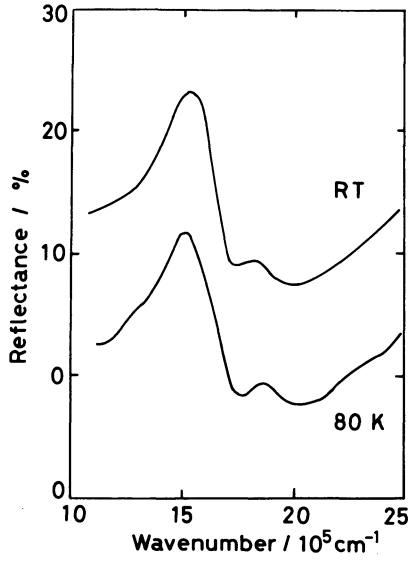


Fig. 5. Reflectance spectrum of the Q-band measured at 80 K and room temperature.

from the comparison of the solution spectra of $Li^+Pc^-$[25] and $Co^{2+}Pc^-$,[26] the ligands of which are oxidized. Since the transition probability of the intramolecular transitions of NiPc cation radicals are small, we consider that these shoulders are faded away at room temperature. The reflectivity of the Q-band of $NiPc(SbF_6)_{0.5}$ is considerably smaller than that of NiPcI.[8] This result is reasonable, since the degree of oxidation $NiPc(SbF_6)_{0.5}$ is larger than that of NiPcI. Thus, the intensity of the Q-band reflects the degree of oxidation at the ligand site. Although a considerable increase of the d-character is expected at 80 K from the $g$-value of the ESR signal, the reflectivity of the Q-band does not change significantly. This result supports again the second case that the majority of carriers are located on the $\pi$-band in the whole temperature range.

We analyzed the reflectance curve of the //c spectrum using the Drude model, and obtained the plasma frequency and the relaxation time. The plasma frequency, $\hbar\omega_P$, was estimated to be 0.86 eV, the relaxation time, $(0.8—1.2)\times10^{-14}$ s, and dielectric constant, 2.1. The bandwidth, $4t$, was calculated using the following equation,

$$4t = \{V_m(\hbar\omega_P)^2\}/\{4e^2c^2\sin(k_fc)\}$$

where $V_m$ is the volume of $(NiPc)(SbF_6)_{0.5}$, $c$ the interplanar distance between the adjacent phthalocyanines, $e$ the unit charge of an electron, and $k_f$ the Fermi wavevector. Since the majority of carrier is located on the ligand chain, the width of the $\pi$-band, 4t is estimated to be 1.1 eV from the values, $V_m=6.524\times10^{-22}$ $cm^3$, $\hbar\omega_p=0.86$ eV, $c=3.22\times10^{-8}$ cm, and $k_fc=3\pi/4$. In the analogous materials like $H_2PcI$, NiPcI, and CuPcI, the conduction bands are made up of $\pi$-orbitals

of ligands. The bandwidth of these materials are 0.84,[2] 1.3,[12] and 1.4 eV[14] for NiPcI, $H_2$PcI, and CuPcI, respectively. The bandwidth, 1.1 eV, of $NiPc(SbF_6)_{0.5}$ falls in the range of these materials with $\pi$-conduction bands. We briefly comment on the relaxation time of conduction electrons which is the measure of the strength of the electron-phonon interaction. Although the ambiguity of the relaxation time is much larger than that of plasma frequency in the curve-fitting analysis, the following discussion is qualitatively reliable. The relaxation time is comparable with the corresponding values, $0.7\times10^{-14}$ s for NiPcI and $0.9\times10^{-14}$ s for $H_2$PcI, and $1.4\times10^{-14}$ s for CuPcI[14] but significantly longer than the room-temperature values of other organic metals, $0.4\times10^{-14}$ s for TTF-TCNQ,[27] $0.2\times10^{-14}$ s for TTF-$I_{0.71}$,[28] $0.3\times10^{-14}$ s for $(TMTSF)_2PF_6$,[29] $0.4\times10^{-14}$ s for $(TMTSF)_2ClO_4$,[30] $0.3\times10^{-14}$ s for $(DMtTSF)_2ReO_4$.[31] These results suggest that the conduction electron on the phthalocyanine ring is interacting weakly with the lattice phonon.

**$NiPc(AsF_6)_{0.5}$.** In contrast to $NiPc(SbF_6)_{0.5}$, we found a strong sample dependence on the magnetic property of $NiPc(AsF_6)_{0.5}$. To characterize these magnetically different crystals, we selected 90 crystals which were larger than 0.05 mm×0.05 mm×6 mm, and measured the ESR signal on each crystal under the condition that the needle axis is perpendicular to the static magnetic field. Figure 6 shows the distribution of the ESR patterns which was classified by the linewidth. The ESR signal is sometimes composed of two or three components with different linewidths. These mixtures are indicated by the dotted histograms. As shown in this figure, the linewidth of the ESR signal is almost continuously distributed from about 1 G to over 100 G (1 G=$10^{-4}$ T). F denotes the sample which is ESR silent probably due to the too broad linewidth. The typical examples of the ESR pattern is shown in Fig. 7. The different types of crystals, i.e. types A and D, were usually found in the same batch. We consider that the sample dependence is not attributed to the contamination of the magnetic impurities because the samples are prepared from the same starting materials as what was used for the preparation of $NiPc(SbF_6)_{0.5}$ which does not show such a sample dependence. The temperature dependence of the magnetic susceptibility, linewidth and g-value of the typical types of crystals were measured on the single crystals of the types A and B and the aligned crystals of the types D and E. The results are shown in Fig. 8.

It is well-known that the electrochemical oxidation of BEDT-TTF (bis(ethylenedithio)tetrathiafulvalene) produces the crystals which have many chemical compositions and a variety of polymorphs with the same composition.[32] In these crystals of BEDT-TTF, the physical properties are quite different from each other. In order to examine whether these ESR patterns

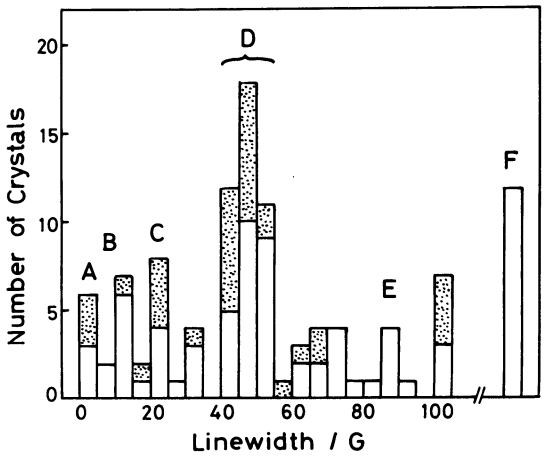


Fig. 6. Histogram of the sample dependence of the ESR signal of $NiPc(AsF_6)_{0.5}$ classified by the linewidth. The open rectangles denote the number of crystals with a single component and dotted ones stands for the ones which exhibit two or three components.

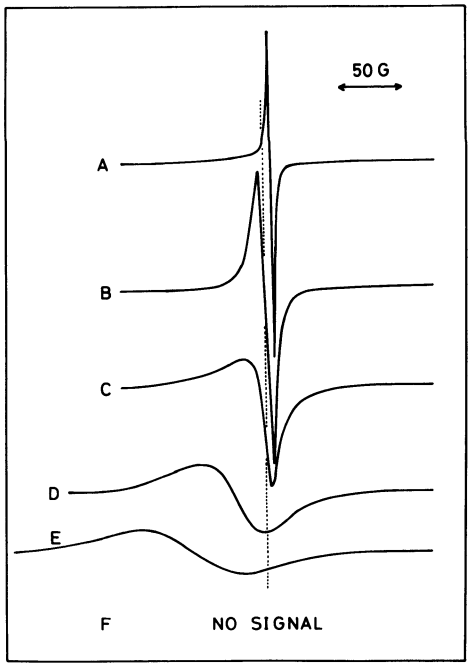


Fig. 7. Line shape of the ESR signal of the typical crystals of $NiPc(AsF_6)_{0.5}$. The symbols, A—F, correspond to those written in Fig. 6.

comes from the different chemical compositions or the polymorphism, we conducted the elementary analysis on each crystals with the aid of EPMA. The results shown in Table 2 indicates that all these crystals have essentially the same chemical composition, 2:1 for Ni:As within the experimental error.

The oscillation and Weissenberg photographs indicated that these crystals belonged to the same orthorhombic system with the space group, *Pncm* or *Pnc*2. The lattice constants of the types A, B, D, and E

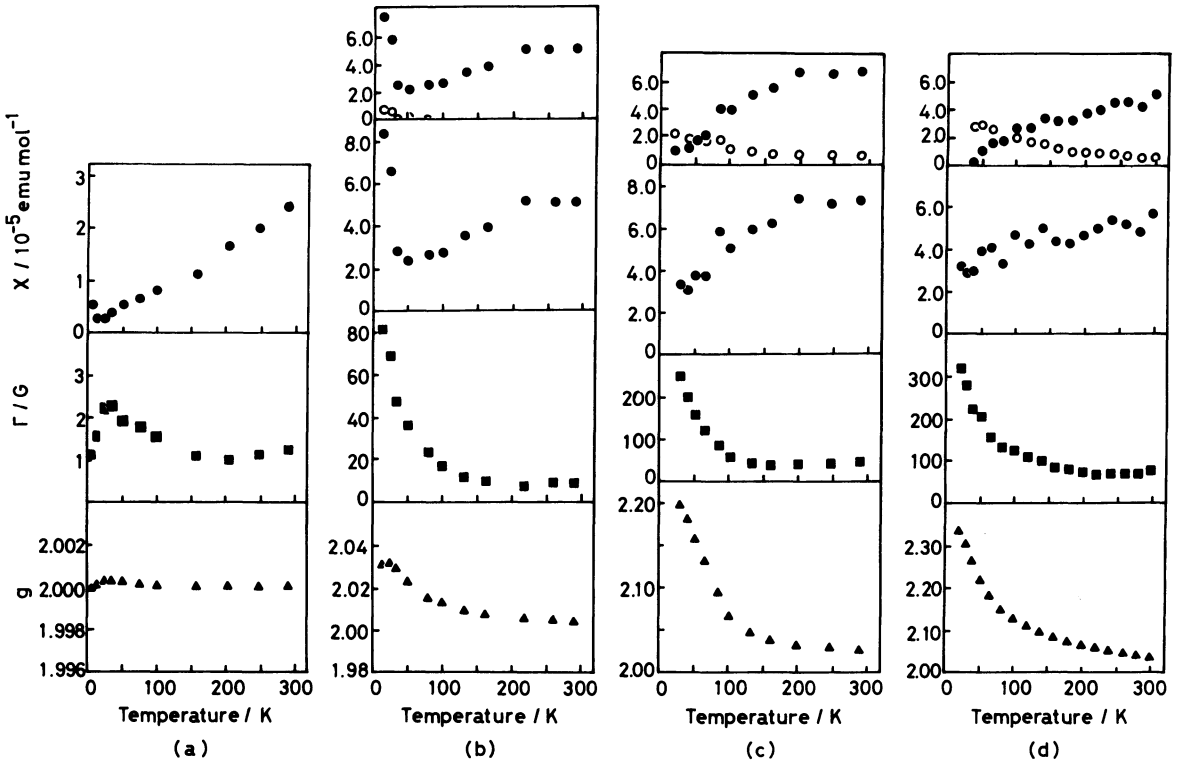


Fig. 8. Divided spin susceptibilities (top panel, solid circle for the Pc chain and open circle for the Ni chain), observed spin susceptibility (second from the top, solid circle), linewidth (second from the bottom, square), and $g$-value (bottom, triangle) of the ESR signal of the (a) type A, (b) type B, (c) type D, and (d) type E crystals of $NiPc(AsF_6)_{0.5}$. Except the type A crystal, the spin susceptibility is calibrated to the absolute value.

Table 2. Elementary Analysis of Ni and As of NiPc-$AsF_6$ Salts by the Method of EPMA

| | A | B | D | E |
|---|---|---|---|---|
| As/Ni | 0.48 | 0.43 | 0.49 | 0.51 |
| $\sigma$ | 0.04 | 0.07 | 0.02 | 0.02 |

Table 3. Lattice Constants of $NiPc(AsF_6)_{0.5}$ and $NiPc(SbF_6)_{0.5}$

| | a | b | c |
|---|---|---|---|
| $NiPc(AsF_6)_{0.5}$ | | | |
| A | 14.015(1) | 28.485(2) | 6.466(3) |
| B | 14.11(2) | 28.37(3) | 6.462(3) |
| E | 14.018(1) | 28.485(2) | 6.468(4) |
| F | 14.027(4) | 28.495(11) | 6.447(6) |
| $NiPc(SbF_6)_{0.5}$[a)] | 14.113(1) | 28.710(2) | 6.441(2) |

a) See Ref. 14.

were determined using a four-circle diffractometer on the crystals of $NiPc(AsF_6)_{0.5}$. The results are shown in Table 3 together with that of $NiPc(SbF_6)_{0.5}$. The lattice constants agreed with each other except that of the type B crystal. We consider that this small difference comes from the poor quality of the crystal B, which is reflected on the 10 times larger standard deviations. The crystal structure analysis was conducted on the type A crystal which exhibits most different magnetic behavior from that of $NiPc(SbF_6)_{0.5}$. The final atomic coordinates are shown in Table 4. Figure 9 illustrates the molecular arrangement in the crystal of NiPc-$(AsF_6)_{0.5}$. The NiPc molecules are slightly zigzag stacking along the c-axis. The shift of the central Ni atom from the axis (0.5, 0.25, z) is 0.21 Å, which is the same value as that of $NiPc(SbF_6)_{0.5}$. The neighboring NiPc is staggered by 40.4° around the stacking axis. The crystal structure is almost exactly the same as that of $NiPc(SbF_6)_{0.5}$.[33] The temperature factors of $AsF_6^-$ is considerably larger than those of NiPc. The root-mean-square displacement of the As atom is 0.23, 0.19, and 0.45Å along the a-, b-, and c-axes, respectively. Since the c-component of the temperature factor of As is also large, $AsF_6^-$ is not only orientationally disordered, but also positionally fluctuated along the c-axis. Therefore, the molecular structure of $AsF_6^-$ is determined to be heavily distorted as shown in Fig. 9a. This kind of distortion was also observed on $SbF_6^-$ in the crystal of $NiPc(SbF_6)_{0.5}$.[15] Incidentally the equivalent isotropic temperature factors of $SbF_6^-$ were 7.8 for Sb and 14.9, 15.2, and 25.9 for F atoms. No significant difference was found in the molecular structure of NiPc between this complex and $NiPc(SbF_6)_{0.5}$. We consider that the structure of the type A crystal is essentially the same as

Table 4. Fractional Atomic Coordinates ($\times 10^4$) and Equivalent Temperature Factors ($B_{eq}=(4/3)\sum_{ij}\beta_{ij}a_ja_i$)

| Atom | X | Y | Z | $B_{eq}$ | Atom | X | Y | Z | $B_{eq}$ |
|---|---|---|---|---|---|---|---|---|---|
| Ni1 | 5123(1) | 2456(1) | 57(8) | 1.8 | C24 | 5910(7) | 1043(4) | 32(44) | 2.4 |
| N2 | 6355(6) | 2734(3) | 22(33) | 1.9 | C25 | 5227(8) | 1427(3) | 108(40) | 2.4 |
| N3 | 5694(5) | 1849(3) | 80(34) | 1.9 | C26 | 3687(7) | 1704(4) | 168(37) | 2.1 |
| N4 | 3893(6) | 2176(3) | 10(34) | 2.0 | C27 | 2662(7) | 1626(4) | 64(40) | 2.3 |
| N5 | 4555(5) | 3058(3) | 16(33) | 1.8 | C28 | 2125(9) | 1213(4) | 219(44) | 3.2 |
| N6 | 7376(6) | 2047(3) | 226(31) | 2.1 | C29 | 1142(9) | 1274(5) | −51(55) | 4.1 |
| N7 | 4296(6) | 1350(3) | −25(35) | 2.5 | C30 | 718(8) | 1712(5) | 118(56) | 4.2 |
| N8 | 2868(6) | 2864(3) | 11(35) | 2.4 | C31 | 1261(8) | 2125(5) | −148(43) | 3.2 |
| N9 | 5951(6) | 3563(3) | −7(34) | 2.1 | C32 | 2250(7) | 2065(4) | 70(42) | 2.5 |
| C10 | 6560(7) | 3207(3) | 146(37) | 2.0 | C33 | 3028(7) | 2405(4) | 92(43) | 2.3 |
| C11 | 7594(7) | 3281(4) | 143(37) | 2.2 | C34 | 3594(7) | 3159(4) | 26(38) | 2.2 |
| C12 | 8144(8) | 3684(4) | −29(48) | 3.1 | C35 | 3443(7) | 3670(4) | 30(42) | 2.3 |
| C13 | 9125(8) | 3625(4) | 35(56) | 4.4 | C36 | 2617(8) | 3937(4) | 59(47) | 3.3 |
| C14 | 9534(8) | 3180(4) | 117(56) | 4.0 | C37 | 2739(10) | 4424(4) | 9(60) | 4.5 |
| C15 | 8983(8) | 2778(4) | −173(40) | 2.7 | C38 | 3646(10) | 4624(4) | 153(62) | 4.4 |
| C16 | 8001(7) | 2844(3) | 72(44) | 2.2 | C39 | 4483(9) | 4355(4) | 247(44) | 3.1 |
| C17 | 7215(6) | 2506(4) | 71(43) | 2.1 | C40 | 4337(7) | 3870(4) | 51(41) | 2.4 |
| C18 | 6651(7) | 1751(3) | 102(41) | 2.2 | C41 | 5027(8) | 3490(3) | 103(41) | 2.2 |
| C19 | 6814(7) | 1240(4) | −4(43) | 2.5 | As42 | 10000 | 5000 | 5000 | 7.6 |
| C20 | 7625(8) | 968(4) | 10(51) | 3.5 | F43 | 9799(30) | 5336(7) | −2059(31) | 22.8 |
| C21 | 7522(10) | 486(4) | 243(52) | 3.9 | F44 | 11029(8) | 5240(4) | −530(63) | 19.0 |
| C22 | 6601(10) | 288(4) | 102(55) | 4.7 | F45 | 9552(8) | 5425(4) | 1559(27) | 8.9 |
| C23 | 5784(9) | 557(4) | 238(47) | 3.2 | | | | | |

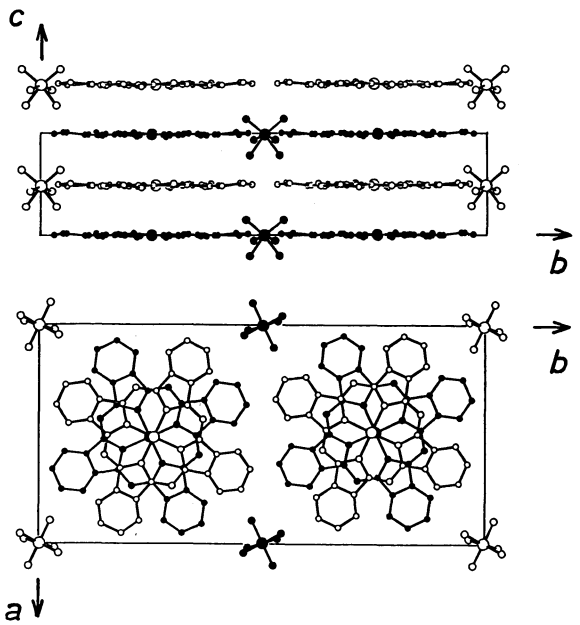


Fig. 9. Crystal structure of $NiPc(AsF_6)_{0.5}$. (a) Side view and (b) top view of NiPc columns.

those of the other types of crystals and of $NiPc(SbF_6)_{0.5}$. The anisotropic temperature factors and $F_o-F_c$ data are deposited as Document No. 8856 at the office of the Editor of Bull. Chem. Soc. Jpn.

The electrical conductivities of the crystals of types C and F exhibited metallic behavior at least down to 200 K. The temperature dependence of the resistivity of these crystals was exactly the same with each other. Due to the resistivity jumps, the intrinsic electrical properties in the low temperature region could not be revealed.

The reflectance spectra of the crystals, C and F, were measured at room temperature. The spectrum of the type C crystal was shown in Fig. 10. These crystals exhibited a typical metallic reflection spectrum with a one-dimensional nature along the c-axis. The reflectivity curve around the plasma edge was analyzed by the use of Drude model. The plasma frequencies and the relaxation times were obtained to be 0.89 eV and $1\times10^{-14}$ s for the type C crystal and 0.91 eV and $0.9\times10^{-14}$ s for the type F crystal. The bandwidth of the tight binding band of these crystals were estimated to be 1.2 eV for both types. The $\perp c$ spectrum was drawn by a dotted line. The dispersions around 15000 $cm^{-1}$ are the Q-band of the neutral NiPc. No significant difference was found between the spectra of the types C and F in the Q-band region. If we use the two-band model, the degree of oxidation at the Ni site of the type F is different from that of the type C. However, the plasma edge and the Q-band of the type C were almost exactly the same as those of the type F. This result is quite similar to the temperature independent property on the Q-band of $NiPc(SbF_6)_{0.5}$.

The crystal structure, electrical conductivity, and reflectance spectrum of $NiPc(AsF_6)_{0.5}$ are essentially the same as those of $NiPc(SbF_6)_{0.5}$. The temperature dependence of g-values and the linewidths of some $NiPc(AsF_6)_{0.5}$ quite resemble those of $NiPc(SbF_6)_{0.5}$, and $NiPc(SbF_6)_{0.5}$ is situated between the types D and E comparing the ESR property of $NiPc(SbF_6)_{0.5}$ with those of $NiPc(AsF_6)_{0.5}$ shown in Fig. 8. Thus, the magnetic

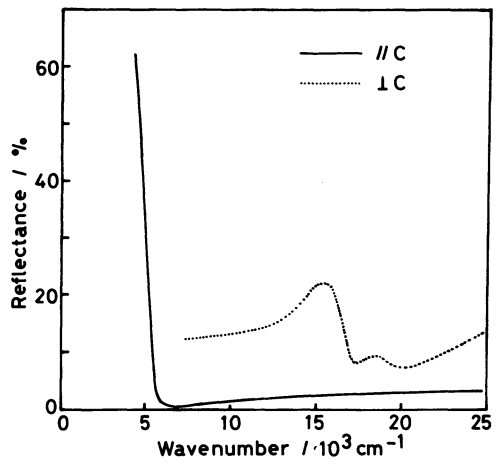


Fig. 10. Polarized reflectance spectrum of the single crystal of $NiPc(AsF_6)_{0.5}$.

properties of $NiPc(AsF_6)_{0.5}$ should be explained on the same basis as $NiPc(SbF_6)_{0.5}$. The spin susceptibilities of these types were divided into the contribution from the Ni chain, $\chi_{Ni}(T)$, and that from the Pc chain, $\chi_{Pc}(T)$, applying the same method as described before. The results are shown in the top panels od Fig. 8. As shown in these figures, $\chi_{Ni}(T)$ increases upon cooling like Curie law. Analyzing the temperature dependence of $\chi_{Ni}(T)$ by the use of the Curie law, the spin concentrations at the Ni site were estimated to be $2\times10^{-4}$, $3\times10^{-3}$, $4\times10^{-3}$ spins per a NiPc for the types B, D, and E. These concentrations are reasonable for the localized spins at i.e. the defect sites. Furthermore, the chemical compositions, lattice parameters, electrical conductivities, and reflectance spectra of $NiPc(AsF_6)_{0.5}$ are sample independent. Therefore, these results support that the oxidation takes place mainly at the ligand site so that the conduction electrons are located on the ligand chain, from the same reason as the temperature independent bulk properties of $NiPc(SbF_6)_{0.5}$. Thus the sample dependence of the ESR properties of $NiPc(AsF_6)_{0.5}$ is understandable from the sample dependent concentration of the local spins at the Ni site. That is to say, the concentration of the local spins at the Ni site increases in order of A, B, C, D, E, and F, and the ESR property of the sample A is mostly reflecting the conduction electrons in the Pc chain. This interpretation is consistent with the fact that the behavior of $\chi(T)$ in the crystal A is qualitatively the same as those of $\chi_{Pc}(T)$ of other crystals, B, D, E, of $NiPc(AsF_6)_{0.5}$, and the concentration of the local spins increases from B to E. Unfortunately, the absolute value of the spin susceptibility of the type A crystal could not be obtained, since the number of crystals in this class was very small. The local spins on the lattice defect seem to be located not only at the Ni site but also at the ligand site. The local spins with narrow linewidth are characterized from the sharp rise at low temperature, and they are found in the crystals of types A and B as shown in the top panels of Figs. 8a and 8b. The broader linewidth of the type B crystal is probably attributed to the exchange interaction with the local spins at the Ni sites. We consider that the rise-up of the ESR intensity below 20 K in the crystals of the types A and B is probably related to the low concentration of the local spins at Ni site. When the concentration of the local spins at Ni sites becomes higher like the crystals of the types D and E, the ESR signal of the local spins at the ligand sites are probably hidden by the exchange interaction with the local spins at Ni sites through the conduction electrons on the ligand chain.

The magnetic properties of $NiPc(AsF_6)_{0.5}$ and $NiPc(SbF_6)_{0.5}$ are different from those of NiPcI, although the one-dimensional structure of the NiPc column is the same among them. This different property is connected with the higher degree of oxidation in $NiPc(AsF_6)_{0.5}$ and $NiPc(SbF_6)_{0.5}$ than in NiPcI, and also with the near orbital energy between the $3d_{z^2}$ orbital of the Ni atom and the HOMO ($a_{1u}$) of the ligand.[5] However, it is not clear at present why such a heavy sample dependence takes place only in the crystals of $NiPc(AsF_6)_{0.5}$, since the different point between $NiPc(AsF_6)_{0.5}$ and $NiPc(SbF_6)_{0.5}$ is only the anion size. If we adopt the model that the conduction electrons are located mainly on the Pc chain, the spin susceptibility on the Pc chain, $\chi_{Pc}(T)$, cannot be the Pauli paramagnetism, since $\chi_{Pc}(T)$ decreases upon the decrease of temperature. We consider that the number of conduction electrons decreases on lowering temperature due to the existence or growing-up of a narrow energy gap. The origin of this narrow gap is either the Peierls instability or the strong electron–electron Coulomb interaction. In the organic metals, the electron–electron Coulomb interaction is estimated from the enhancement of the spin susceptibility as compared with the Pauli paramagnetic susceptibility calculated from the transfer integrals which is obtained from the optical spectrum.[34] The spin susceptibility, $\chi_{Pc}(T)$, was roughly estimated from the flat region of $\chi_{Pc}(T)$. They are $8\times10^{-5}$ emu mol$^{-1}$ at room temperature for $NiPc(SbF_6)_{0.5}$ and $(5-7)\times10^{-5}$ emu mol$^{-1}$ at room temperature for the crystals of types B, D, and E. The Pauli paramagnetic susceptibility ($\chi_{Pauli}$) was calculated to be $5\times10^{-5}$ emu mol$^{-1}$ for all the crystals of $NiPc(AsF_6)_{0.5}$ and $NiPc(SbF_6)_{0.5}$. Therefore, the enhancement factor, $\chi_{s,obs}/\chi_{Pauli}$, is significantly smaller than the corresponding values, 3.0 for TTF-TCNQ and 3.3 for $TMTSF(PF_6)_{0.5}$.[34] Therefore, the Coulomb interaction on the Pc chain is considered to be weak, so that Peierls distortion may be one of the candidates for the energy gap.

The crystals of $NiPc(SbF_6)_{0.5}$ and $NiPc(AsF_6)_{0.5}$ belong to the orthorhombic system, wheres the crystals of NiPcI and $NiPc(ClO_4)_{0.39-0.47}$ to the tetragonal

system. This structural difference comes from the shape and the position of the counter anions. In the case of the NiPcI crystal, the periodicity of the linear $I_3^-$ does not coincide with that of NiPc, so that the $I_3^-$ is only ordered one-dimentionally along the stacking axis. The tetrahedral $ClO_4^-$ is located at the interstitial position of the molecular layers of NiPc with the site occupancy of about 0.5. Therefore, in both crystals the counter anions are positionally disordered. On the other hand, the $SbF_6^-$ and $AsF_6^-$ are located at the same plane as the molecular layer of NiPc. This location of the anion brings about the two zigzag chains in the unit cell. Thus the unit cell contains two channels for accommodating the counter anions, so that these anions are three-dimensionally ordered. The difference of the periodic potential may affect the electronic conduction along the one-dimensional NiPc column at low temperature. According to Martinsen et al., the electrical conductivity of NiPcI exhibits an extrinsic peak around 20—30 K, and the Peierls instability is suppressed by the random potential.[8] From this viewpoint, it is interesting to examine the low temperature behavior of the electrical resistivity of $NiPc(SbF_6)_{0.5}$ and $NiPc(AsF_6)_{0.5}$. Unfortunately, the electrical conductivity of these material in the low temperature region is unidentified at present because of the occurrence of frequent resistivity jumps.

We acknowledge Professor Hiroki Haraguchi in the Chemistry Department of the University of Tokyo for conducting the ICP atomic emission spectroscopy. We thank Professor Akimasa Masuda, Dr. Hiroshi Shimizu, and Dr. Kazuya Takahashi in the Chemistry Department of the University of Tokyo for the assistance of the elementary analysis by the method of EPMA. We acknowledge Dr. Kosuke Ueyama, in Kuroda Solid Surface Project, in JRDC, for making a micro-diaphragm to eliminate the stray X-ray. This research was supported by the Ciba-Geigy Foundation for the Promotion of Science (Grant 104269 to K. Y.).

**References**

1) J. Martinsen, L. J. Pace, T. E. Phillips, B. M. Hoffman, and J. A. Ibers, *J. Am. Chem. Soc.*, **104**, 83 (1982).

2) C. J. Schramm, R. P. Scaringe, D. R. Stojakovic, B. M. Hoffman, J. A. Ibers, and T. J. Marks, *J. Am. Chem. Soc.*, **102**, 6702 (1980).

3) A. M. Schaffer, M. Gouterman, and E. R. Davidson, *Theor. Chim. Acta*, **30**, 9 (1973).

4) M.-H. Whangbo and K. R. Stewart, *Isr. J. Chem.*, **23**, 133 (1983).

5) F. W. Kutzler and D. E. Ellis, *J. Chem. Phys.*, **84**, 1033 (1986).

6) W. A. Little, *J. Phys. (Paris) Colloq.*, **1983**, C3-819.

7) T. E. Phillips, R. D. Scaringe, B. M. Hoffman, and J. A. Ibers, *J. Am. Chem. Soc.*, **102**, 3435 (1980).

8) J. Martinsen, S. M. Palmer, J. Tanaka, R. L. Greene, and B. M. Hoffman, *Phys. Rev. B*, **30**, 6269 (1984).

9) S. M. Palmer, J. L. Stanton, N. K. Jaggi, B. M. Hoffman, J. A. Ibers , and L. H. Schwartz, *Inorg. Chem.*, **24**, 2040 (1985).

10) J. Martinsen, J. L. Stanton, R. L. Greene, J. Tanaka, B. M. Hoffman, and J. A. Ibers, *J. Am. Chem. Soc.*, **107**, 6915 (1985).

11) T. Inabe, S. Nakamura, W. B. Liang, T. J. Marks, R. L. Burton, C. R. Kannewurf, and K. Imaeda, *J. Am. Chem. Soc.*, **107**, 7224 (1985).

12) T. Inabe, T. J. Marks, R. L. Burton, J. W. Lyding, W. J. McCarthy, C. R. Kannewurf, G. M. Reisner, and F. H. Herbstein, *Solid State Commun.*, **54**, 501 (1985).

13) M. Almeida, M. G. Kanatzidis, L. M. Tonge, T. J. Marks, H. O. Maracy, W. J. McCarthy, and C. R. Kannewurf, *Solid State Commun.*, **63**, 457 (1987).

14) M. Y. Ogawa, J. Martinsen, S. M. Palmer, J. L. Stanton, J. Tanaka, R. L. Greene, B. M. Hoffman, and J. A. Ibers, *J. Am. Chem. Soc.*, **109**, 1115 (1987).

15) K. Yakushi, M. Sakuda, H. Kuroda, A. Kawamoto, and J. Tanaka, *Chem. Lett.*, **1986**, 1161.

16) K. Yakushi, M. Sakuda, I. Hamada, H. Kuroda, A. Kawamoto, J. Tanaka, T. Sugano, and M, Kinoshita, *Synthetic Metals*, **19**, 769 (1987).

17) J. M. Assour and W. K. Kahn, *J. Am. Chem. Soc.*, **87**, 207 (1965).

18) H. Oyanagi, T. Matsushita, M. Ito, and H. Kuroda, *KEK Report*, **83**, 30 (1984).

19) K. Yakushi, M. Iguchi, and H. Kuroda, *Bull. Chem. Soc. Jpn.*, **52**, 3180 (1979).

20) A. P. Bobrovskii and A. N. Sidorov, *J. Struct. Chem. (Engl. Transl.)*, **17**, 50 (1976).

21) J. S. Griffith, *Discuss. Faraday Soc.*, **26**, 81 (1958).

22) Y. Tomkiewicz, A. R. Taranko, and J. B. Torrance, *Phys. Rev.*, **36**, 751 (1976).

23) J. E. Hahn, R. A. Scott, K. O. Hodgson, S. Doniach, S. R, Desjardins, and E. I. Solomon, *Chem. Phys. Lett.*, **88**, 595 (1982).

24) These results are probably attributable to the different orbital relaxation effects on the 1s to 3d excited states.

25) P. Turek, J.-J. Andre, A. Giraudeau, and J. Simon, *Chem. Phys. Lett.*, **134**, 471 (1987).

26) P. C. Minor, M. Gouterman, and A. B. P. Lever, *Inorg. Chem.*, **24**, 1894 (1985).

27) Y. Cao, K. Yakushi, and H. Kuroda, *Solid State Commun.*, **35**, 739 (1980).

28) Y. Cao, K. Yakushi, and H. Kuroda, *Solid State Commun.*, **35**, 601 (1980).

29) C. S. Jacobsen, D. B. Tanner, and K. Bechgaard, *Phys. Rev. B*, **28**, 7019 (1983).

30) K. Kikuchi, I. Ikemoto, K. Yakushi, H. Kuroda, and K. Kobayashi, *Solid State Commun.*, **42**, 433 (1982).

31) K. Kikuchi, K. Yakushi, H. Kuroda, I. Ikemoto, and K. Kobayashi, *Mol. Cryst. Liq. Cryst.*, **125**, 345 (1985).

32) R. P. Shibaeva, V. F. Kaminshii, and E. B. Yagubskii, *Mol. Cryst. Liq. Cryst.*, **119**, 361 (1985).

33) We revised the lattice constants and the space group of $NiPc(AsF_6)_{0.5}$, since the weak reflections ($hkl$) with $k=2n+1$ were missing in the data collection of the previous paper.

34) C. S. Jacobsen, *J. Phys. C*, **19**, 5643 (1986).